JGR Space Physics

RESEARCH ARTICLE
10.1029/2025JA034820

Reduced Geomagnetic Shielding During the Laschamps Excursion and Its Impact on Cosmic-Ray-Induced Atmospheric Radiation

N. Larsen[1,2], I. Usoskin[1,2], A. Mishev[2], S. Koldobskiy[2], and P. Väisänen[2]

[1]Institute for Space-Earth Environmental Research, University of Nagoya, Nagoya, Japan, [2]Space Physics and Astronomy Research Unit, and Sodankylä Geophysical Observatory, University of Oulu, Oulu, Finland

Key Points:

- Global apparent geomagnetic cut-off rigidities were computed for the Laschamps excursion using the LSMOD.2 paleomagnetic field model
- Radiation doses at aviation altitude were computed using the CRAC: DOMO radiation model under various conditions throughout the excursion
- Complex magnetic field configuration increased radiation at low latitudes and reduced it at high latitudes during the weakest dipole phase

Supporting Information:

Supporting Information may be found in the online version of this article.

Correspondence to:

N. Larsen,
larsen.nicholas.peter.d8@f.mail.nagoya-u.ac.jp;
nicholas.larsen@oulu.fi;
nlarsen1505@gmail.com

Citation:

Larsen, N., Usoskin, I., Mishev, A., Koldobskiy, S., & Väisänen, P. (2026). Reduced geomagnetic shielding during the Laschamps excursion and its impact on cosmic-ray-induced atmospheric radiation. *Journal of Geophysical Research: Space Physics*, *131*, e2025JA034820. https://doi.org/10.1029/2025JA034820

Received 27 OCT 2025
Accepted 8 FEB 2026

Author Contributions:

Conceptualization: I. Usoskin
Data curation: N. Larsen
Investigation: N. Larsen
Methodology: N. Larsen
Software: N. Larsen, A. Mishev
Writing – original draft: N. Larsen, I. Usoskin, A. Mishev, S. Koldobskiy, P. Väisänen
Writing – review & editing: N. Larsen, I. Usoskin, A. Mishev, S. Koldobskiy, P. Väisänen

Abstract The Laschamps geomagnetic excursion (≈41,000 years BP) was a period of significant weakening and incomplete reversal of the Earth's magnetic field. The weakening substantially reduced geomagnetic shielding against cosmic rays (CRs), which contribute to phenomena at Earth, such as cosmogenic isotope production, and atmospheric ionisation and radiation. In this work, we expand upon previous modeling of geomagnetic shielding during excursions and provide a robust methodology for assessing the CR impacts during such an event, focusing on CR-induced atmospheric radiation. This was achieved by updating the open-source OTSO CR trajectory tool to allow for paleomagnetic field models, namely LSMOD.2, to be used as inputs to compute global apparent geomagnetic cut-off rigidities at 100-year intervals throughout the excursion. The CRAC:DOMO model was used to assess the CR-induced atmospheric radiation, and the potential impact on the aviation industry was investigated by computing the effective dose rates for two representative flights, Helsinki to New York and Helsinki to Dubai, under various conditions. Results suggest low-latitude flights, normally well shielded under modern conditions, can experience significant increases in dose rates; in contrast, some high-latitude flight routes may observe decreases in radiation exposure due to the irregular geomagnetic structure during the excursion. These findings reveal that geomagnetic excursions can greatly enhance the levels of CR-induced atmospheric radiation, with wider implications that excursion events can likewise significantly affect other CR-induced processes, such as cosmogenic isotope production and atmospheric ionization. The methodology provided here outlines a framework under which CR impacts can be assessed under non-standard geomagnetic conditions.

1. Introduction

Interstellar and heliospheric space is populated by energetic charged particles known as cosmic rays (CRs), with the majority of high-to ultra-high energy (up to EeV) CRs being of galactic and extragalactic origin, collectively called galactic cosmic rays (GCRs). The current paradigm is that GCRs with energy below 10^{16} eV are accelerated mostly by supernova remnants throughout the galaxy, after which they diffuse and scatter and become effectively isotropic when observed near Earth (Gaisser et al., 2016). GCRs are omnipresent near Earth, with the lower-energy flux (CRs with energy below ≈30 GeV) subjected to solar modulation within a few tens of per cent over the solar activity cycle (Potgieter, 2013). A local source, that is, within the solar system, of lower-energy CRs is the Sun, which can occasionally accelerate solar energetic particles (SEPs) up to energies of several GeVs, during strong eruptive events, with the two main acceleration mechanisms currently believed to be magnetic reconnection at the flare site and magnetic shock front acceleration (Desai & Giacalone, 2016). Such processes can generate solar particle events (SPEs) and, due to the proximity of their source to Earth, they can exhibit strong anisotropies and significantly higher fluxes than GCRs (Klein & Dalla, 2017). Whether SEPs can arrive at Earth depends on the eruption site's magnetic connectivity to Earth, coronal mass ejection shock front expansion, and ambient heliospheric conditions (Gopalswamy et al., 2012, 2014). It is also not guaranteed that large solar eruptions will produce SEPs, and work is currently ongoing in developing models to predict which eruptions can produce SEPs (Papaioannou et al., 2025). These factors combined mean that large SPEs with a noticeable impact on Earth are quite sporadic in nature.

Upon arriving at Earth, CRs interact with its magnetic field, which acts as a protective barrier, except at the poles where little protection is offered. Incoming charged CRs are subjected to the Lorentz force upon arrival at the Earth's magnetosphere, causing most low-energy CRs to be deflected away from Earth. CRs with enough energy can overcome this geomagnetic shielding effect and arrive in the Earth's atmosphere (Dorman, 2004). The energy

required for CRs to penetrate the geomagnetic field depends on the arrival location and direction of incidence of the CR and geomagnetospheric conditions. It is conveniently quantified by the term rigidity, or particle's momentum per unit charge, given in units GV. Rigidity is a CR species-independent term that quantifies the effect of a magnetic field on a charged particle's motion: the higher the rigidity value, the less deflected the particle's trajectory (Cooke et al., 1991). The term "cut-off rigidity" (R_c) is often used to introduce the threshold rigidity needed by a CR to penetrate the magnetosphere and arrive at a given location at the Earth's surface. Under the current geomagnetic conditions, the cut-off rigidity values range from ≈0 GV in polar regions up to ≈17 GV in equatorial regions (Gerontidou et al., 2021). CRs can therefore gain easier access to the Earth's polar regions, enhancing their impacts there.

While the Earth's magnetic field is currently dominated by a slightly tilted eccentric dipolar structure, this has not always been the case. The geomagnetic field varies over time, with fluctuations ranging from fast disturbances, caused by solar wind and the interplanetary magnetic field (Pulkkinen, 2007), to gradual shifts that span millennia, caused by the internal geodynamo (Buffett, 2000). In Earth's past, rare polarity reversals, where the north and south poles of the dipole switch, and excursions, weakening of the dipole field without polarity reversal, took place irregularly. The most recent and well-studied geomagnetic excursion is the Laschamps event about 41 millennia ago (Guillou et al., 2004; Panovska et al., 2019). The magnetic field structure during such events can become increasingly complex and essentially non-dipole. The weakening of the Earth's dipole moment can decrease the overall geomagnetic shielding provided by the Earth, increasing the impacts posed by CRs on the terrestrial environment. Excursion and reversal events are still poorly understood, mainly due to the lack of quality paleomagnetic samples required to study Earth's historic magnetic field (Roberts, 2008). However, in recent years, significant progress has been made in developing magnetic field models for the Earth's past using such paleomagnetic data sets (Constable et al., 2016; Korte et al., 2019; Panovska et al., 2018, 2021).

SPEs that produce SEPs with enough energy and flux to penetrate the geomagnetic shielding provided by the Earth and be detected by ground-based instruments, such as neutron monitors, in statistically significant quantities are called ground-level enhancement (GLE) events (for details see Aschwanden, 2012; Poluianov et al., 2017; Shea & Smart, 1982). GLEs indicate the most powerful solar eruptions and can cause severe space weather effects (for details see Miroshnichenko, 2018, and references therein). CRs that arrive at Earth induce various effects, with some having negative consequences on human health and technology. Some notable CR-induced effects are cosmogenic isotope production, single-event effects in electrical systems (Pulkkinen, 2007), and enhanced atmospheric ionisation and radiation levels. The impacts of CRs are controlled by CR flux and energy, and the level of atmospheric and geomagnetic shielding present at a location on Earth. In the case of atmospheric radiation, which is explicitly considered in this work, atmospheric shielding decreases with increasing altitude, resulting in higher radiation doses at aviation altitudes. Additionally, the reduction in geomagnetic shielding as you approach the poles permits higher fluxes of CRs to access, posing a salient issue for high-latitude and polar flights (Shea & Smart, 2012). Indirect proxy records, such as the aforementioned cosmogenic isotopes, indicate that extreme solar particle events (ESPEs) can rarely, roughly once per millennium, occur with the SEP flux being several orders of magnitude stronger than observed during "regular" GLEs (Cliver et al., 2022; Usoskin et al., 2023). ESPEs are typically considered when investigating the worst-case space weather radiation scenarios.

Here, we perform detailed modeling by applying the most up-to-date models and data sets of the possible impact of a geomagnetic field weakening, exemplified by the Laschamps excursion, on the radiation environment in the Earth's atmosphere, especially at aviation altitudes. In doing so, we provide a robust methodology for examining other CR-induced impacts during periods of significant geomagnetic weakening and non-standard magnetic field configurations.

2. Laschamps Excursion

In the 1960s, studies into the Laschamps and Olby lava flows revealed geomagnetic anomalies. The historical geomagnetic field structure is preserved in volcanic rocks by ferrous minerals (e.g., iron-bearing minerals) that align with the geomagnetic field at the time of eruption, and become locked in place as the lava cools and solidifies. The ferrous materials in the studied lava flows showed a short-lived geomagnetic reversal event (excursion event), which was then dubbed the Laschamps excursion event. The axial dipole moment reversed polarity and decreased to around 5% of its current-day strength during the deep phase of the event, but then

returned to normal (Panovska et al., 2021). Recent dating has determined that the Laschamps excursion occurred ≈41 millennia ago (Korte et al., 2019).

The Earth's magnetic field is typically expressed using a set of spherical harmonic expansion coefficients (Alken et al., 2021), also known as Gaussian coefficients, which can be used to express a scalar potential at a given location on the Earth. The expression of the scalar potential (V) is shown in Equation 1

$$V(r,\theta,\phi,t) = a\sum_{n=1}^{N}\sum_{m=1}^{n}\left(\frac{a}{r}\right)^{n+1}\cdot\left[g_n^m(t)\cos(m\phi) + h_n^m(t)\sin(m\phi)\right]P_n^m\cos(\theta) \quad (1)$$

where r,θ,ϕ are geocentric spherical coordinates, t is time, a is the mean radius of the Earth (6,371.2 km), N is the degree of spherical harmonic expansion, n, m are the degree and order respectively, g_n^m, h_n^m are the spherical harmonic coefficients (Gauss coefficients), and $P_n^m\cos(\theta)$ represent the Schmidt semi-normalized Legendre functions (Schmidt, 1917). Modern models, such as the international geomagnetic reference field (IGRF), use this method and take ground-based magnetometer and satellite measurements to derive the Gauss coefficients (Alken et al., 2021). Work by Brown et al. (2018), later improved upon by Korte et al. (2019), used paleomagnetic data from around the globe to derive the Gauss coefficients up to the 10th degree for the Earth's magnetic field during the period 50 to 30 ka before present (BP), where the "present" refers to the start of the year 1950, viz. 00 UT of 01-Jan-1950. The resulting Gauss coefficients make up the LSMOD.2 model; named for the fact that the magnetic field model covers the period of two geomagnetic excursion events, Laschamps (≈41 ka BP) and Mono Lake (≈34 ka BP). We focus on the Laschamps event, which is the most well-studied geomagnetic excursion/reversal with approximate estimates of its terrestrial impact (e.g., Arsenović et al., 2024). However, those previous studies considered an oversimplified approach, assuming the complete absence of the geomagnetic field during the deep phase of the Laschamps event, which is not correct (cf. Mukhopadhyay et al., 2025). Here, we consider a realistic geomagnetic field configuration as described by the Gauss coefficients.

3. Geomagnetic Shielding Reconstruction

To compute the shielding effect of the geomagnetic field, we used the classical method of backtracing particle trajectories (Shea et al., 1965). CR trajectories are simulated backwards from a start location on the Earth's surface, typically starting at 20 km in altitude, until they either enter the interplanetary medium (arrive at the magnetopause boundary) or fail to leave the magnetosphere; such trajectories are known as allowed and forbidden, respectively. Cut-off computations involve the simulation of many trajectories of CRs with varying particle rigidity, leaving from a given location. Through this process, especially in mid-to-high latitude regions, the transition from allowed to forbidden trajectories, as CR rigidity decreases, can be complicated, with a mixture of allowed and forbidden trajectories being present over a rigidity range; this is known as the penumbra. The effective geomagnetic cut-off is used to resolve the complex penumbra revealed during the trajectory tracing methodology and provide a useful quantitative value. Assuming that rigidities are being tested over a range starting at the highest rigidity and decreasing the rigidity in increments, the effective cut-off is computed using Equation 2

$$R_c = R_U - \sum_{R_L}^{R_u}\Delta R_i \text{ (allowed)} \quad (2)$$

where R_c is the effective cut-off rigidity, R_U is the upper cut-off rigidity (the allowed rigidity value above the highest forbidden value), R_L is the lower cut-off rigidity (the lowest allowed rigidity value), ΔR_i is the rigidity step size, (allowed) signifies summation of only allowed rigidity values over the penumbra region (Cooke et al., 1991). The first realistic computation of the geomagnetic shielding during the Laschamps excursion was performed by Gao et al. (2022), who calculated the vertical effective geomagnetic cut-off, using the CR trajectory tracing program created by Smart and Shea (2001). However, the validity of that approach, especially in the vertical cut-off approximation, for a very irregular non-dipole magnetic field configuration is unknown. Here we further develop this approach by applying robust up-to-date methods and a more realistic computation of R_c. To reconstruct the geomagnetic shielding present at the time of the Laschamps excursion, we used the newly developed open-source OTSO tool, which performs numerical backtracking methods to compute CR trajectories

within the Earth's magnetosphere (for details see Larsen et al., 2023). For this work, OTSO was updated to support magnetic field models quantified by the spherical harmonic expansion of a scalar potential and allow lists of Gaussian coefficients as inputs. This enabled the direct use of the LSMOD.2 model. This OTSO update also opens up the possibility of using OTSO to study other periods with unusual geomagnetic field configurations where geomagnetic models are available, such as the aforementioned Mono Lake excursion.

Additionally, OTSO was updated to utilize a rigidity scan method to speed up cut-off computations, and adopted the apparent cut-off ring approximation methodology for use (Bieber et al., 1997), in contrast to the simplified vertical cut-off used by Gao et al. (2022) when generating the planetary cut-off data set over the Laschamps excursion. Here, we note that the cut-off rigidity for a location is also dependent on the arrival direction of the incoming CR. The vertical cut-off rigidity, this being the cut-off for CRs arriving from the zenith, is generally taken as a good approximation of the effective cut-off rigidity, and favored over other methods due to its computational speed (Shea & Smart, 2000). However, the vertical approximation can be imprecise for a weak non-dipole field. The apparent cut-off accounts for the different arrival directions of CRs at the location of interest and provides a more realistic effective cut-off value, though it is significantly more computationally taxing. Adapting OTSO in such a way to include these new methods ensures that the only difference between the two tools is the numerical integrator technique that resolves the equations of motion of the charged particles, allowing for easy comparison between the two tools.

Within OTSO, there are several integrator methods available; in this work, the Vay integrator was used (Vay, 2008) due to its computational speed. The Vay integrator method is a modified version of the Boris integrator, which was recently verified for cut-off computations (Kruchinin et al., 2024). This modification is designed to tackle applied electric fields better than the base Boris method and gives comparable results to other validated integrators in the absence of an applied electric field (Ripperda et al., 2018). Electric fields are typically neglected in cut-off computations under the assumption that the magnetosphere is highly conductive (Bütikofer, 2018). Within OTSO, the step sizes during the integration are defined based on the gyration period of the CR at the given point in the magnetosphere, allowing for smaller steps near the Earth and larger ones further away. In this work, the maximum time step was set to 30% of the gyration period; however, OTSO checks throughout the computation for accruing errors and if, in the process of one step, the CR's kinetic energy changes by more than 0.001% the time step is halved and the integration step is repeated. If the error is less than 0.00001%, the time step is allowed to grow by 10%, this way, OTSO finds an optimal balance between computation speed and accuracy. In Gao et al. (2022), the selected integrator is the Bulirsch-Stoer integration method for the 4^{th}-order Runge-Kutta technique (Stoer & Bulirsch, 2002) with a step size defined as 1% of the gyroradius.

OTSO was used to compute the apparent cut-off using the Bieber et al. (1997) ring approximation method across the globe using a $5° \times 5°$ grid. The rigidity range over which trajectories were computed was 20–0 GV with 0.01 GV steps. A rigidity scan was applied, where steps of 0.5 GV were done first to find rough values of the upper and lower cut-off rigidities. Computations of the CR backwards trajectories started at 20 km above the Earth's surface and concluded whether the particle hit a 25 Earth radii (R_E) sphere surrounding the Earth, roughly representing the magnetopause boundary, returned to Earth, or traveled more than 100 R_E without meeting any of the two prior conditions. Global maps of the cut-off values were computed at 100-year intervals between 48350 and 35650 BP using LSMOD.2 G coefficients as inputs to the magnetic field model, the resulting data can be found in the electronic supplement. Note that due to the extremely distorted nature of the Earth's magnetic field at the time of the excursion event, the application of any external magnetospheric magnetic field models, such as the Tsyganenko models, is invalidated and, as such, has been omitted from the computations. Magnetohydrodynamic simulations should be conducted in the future to model the magnetospheric currents and their associated magnetic fields during the Laschamps excursion event; this is outside the scope of this study.

The computed global cut-offs during the deep phase of the Laschamps excursion (40950 BP) obtained in this work and by Gao et al. (2022) are shown in Figure 1 for visual comparison. The epoch of 40950 BP is taken as the deep phase of the excursion as it corresponds with the minimum dipole moment of $0.386 \cdot 10^{22}$ A m^2, which is approximately 5% of the modern dipole moment ($7.7 \cdot 10^{22}$ A m^2 for the IGRF epoch 2020— Alken et al., 2021). As seen, the structure of the Earth's magnetic field was non-dipole during the deep phase of the Laschamps excursion. While the configuration of the R_c appears similar for the two methods (panels A and B), by OTSO and by Gao et al. (2022), a small systematic discrepancy between them can be observed (see panel C). The latter method may slightly, by up to 0.2 GV, underestimate the cut-off regionally. Some small anomalous regions of

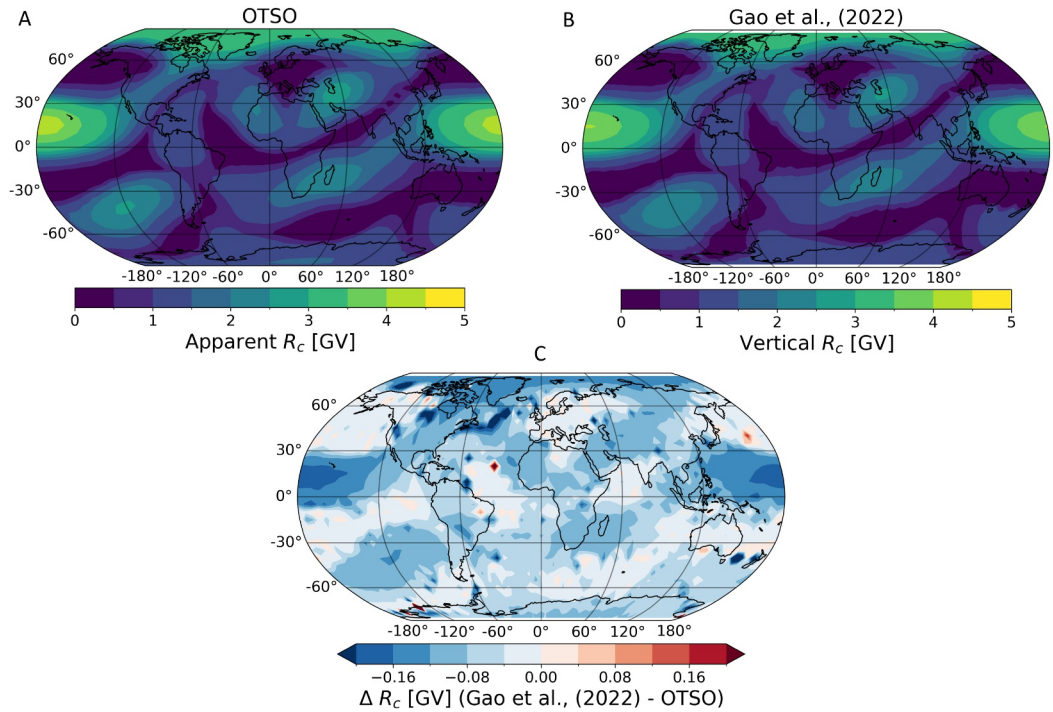

Figure 1. Global cut-off rigidity computation results for the deep phase of the Laschamps Excursion (40950 BP) from this work and Gao et al. (2022), panels (a and b) respectively. Plot (c) is the difference between the two cut-off models.

greater difference (dark red and blue spots in panel C) are ascribed to differences in the integration method applied during the trajectory tracing. More details on these differences can be seen in Appendix A. We confirm that the difference between the apparent (panel A) and vertical (panel B) cut-off rigidity is small during the deep phase of the excursion due to the reduced geomagnetic field strength, as was noted by Gao et al. (2022).

4. Space Weather Application

4.1. Radiation Doses at Aviation Altitude

The weakened geomagnetic field during the excursion allows incoming CRs easier access into the magnetosphere and, subsequently, the atmosphere. Under modern conditions, areas of higher CR-induced effects are normally more localized to the low-cut-off rigidity polar regions, but during geomagnetic excursions and reversals can become more globally pervasive. While we are well protected on the ground by the thick atmosphere, the level of CR-induced radiation can be much higher at aviation altitudes (Beck, 2009; Pelliccioni, 2000; Spurny et al., 1996). This is particularly important in regions with weak geomagnetic shielding, where only the atmospheric shielding remains.

To investigate the impact the Laschamps excursion would have on atmospheric radiation levels, we evaluated the resulting radiation exposure at aviation altitudes. Two representative flight routes were selected for study: a transpolar and a meridional one. The former is the flight from Helsinki to New York (HEL-JFK), and the other from Helsinki to Dubai (HEL-DUB), with flight times of approximately 8.5 and 7.0 hr, respectively. These two flights have been selected because of their very different geomagnetic shielding profiles under modern conditions; with HEL-JFK being a mostly longitudinally varying flight path with low geomagnetic shielding over the North Atlantic, and HEL-DUB being a mostly latitudinally varying flight path with higher geomagnetic shielding. Both of these flight paths were approximated using great circles, as can be seen in Figure 2, and a flight altitude of 40 kft was assumed for the flight's entirety.

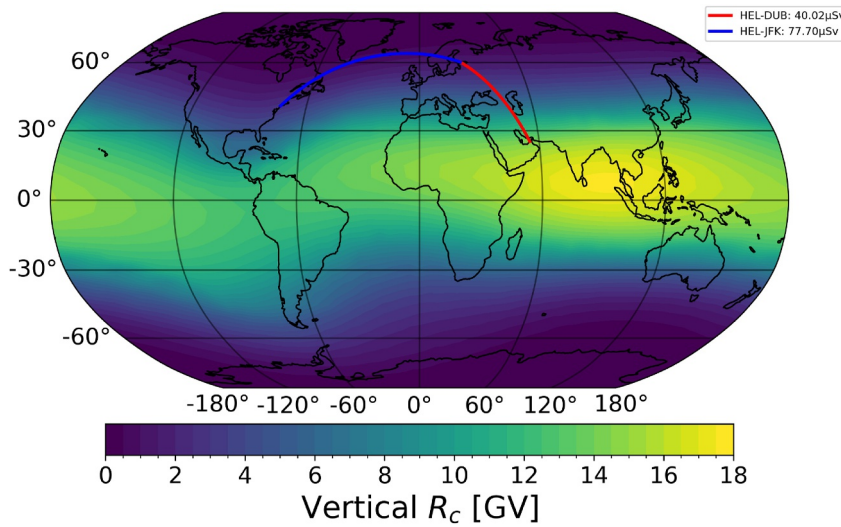

Figure 2. Global map of geomagnetic cut-off values computed by OTSO using the 2020 epoch of the IGRF model. Great-circle flight paths for the HEL-JFK and HEL-DUB flights analyzed in this work are superimposed. The effective dose rate received along each flight at 40 kft (12.19 km) as a result of GCRs, assuming moderate solar activity with a solar modulation potential of 500 MV is provided in the legend.

4.2. CRAC:DOMO

Herein, for the computation of the effective dose, we employed an updated 3-D numerical model CRAC:DOMO (Cosmic Ray Atmospheric Cascade: Dosimetric Model). The model belongs to the family of verified CRAC models based on the full Monte Carlo simulation of the CR-induced atmospheric cascade (e.g., Usoskin et al., 2024; Usoskin & Kovaltsov, 2006). It is among the new generation radiation models (e.g., Copeland et al., 2008; Latocha et al., 2009; Matthiä et al., 2008; Mertens et al., 2013, 2025; Sato et al., 2008), namely a full target approach based on Monte Carlo simulations, that is, simulation of propagation of high-energy particles, protons and α-particles in the Earth's atmosphere. We note that in the model of Mertens et al. (2025), heavier CR species up to $Z = 92$ were also explicitly considered, which, as they note, can provide a non-negligible impact on radiation at aviation altitudes. The full description of the model and applications, including updated look-up tables, are given elsewhere (Larsen & Mishev, 2023; Mishev et al., 2021; Mishev & Usoskin, 2015). CRAC:DOMO employs a response matrix approach (e.g., Hands et al., 2022), that is, yield functions, which represent the dosimetric response, that is, the effective dose, in a given atmospheric layer against a monoenergetic unit flux of primary particles. The yield function is computed separately for protons and α-particles, the latter might also effectively represent heavier CR species (Mishev & Velinov, 2014; Usoskin & Kovaltsov, 2006). The computations were performed employing a GEANT 4 tool (Agostinelli et al., 2003; Desorgher et al., 2005), neglecting the geomagnetospheric effects on cascade development similarly to Wissing and Kallenrode (2009) and assuming starting altitude of incoming CRs, the top of the atmosphere, that is, 100 km above sea level, similarly to Usoskin and Kovaltsov (2006), which is a reasonable approach for aviation altitudes (for details see Mishev & Velinov, 2014, and the discussion therein).

This means that for every altitude and energy level, there are two yield functions produced, one for protons and another for heavier CR species. It represents the integral product of secondary CR particle flux with the fluence-to-dose conversion coefficients $C_j(T^*)$, the latter adopted from the isotropic irradiation model (for details see last columns in the Annex A Tables in Petoussi-Henss et al., 2010). The CRAC:DOMO model agrees with similar models and experimental records (for details see Meier et al., 2016; Meier et al., 2018; Mishev, Tuohino et al., 2018, Mishev, Usoskin et al., 2018; Mishev et al., 2022), and was recently employed for analysis of GLEs (Larsen & Mishev, 2023, 2024, 2025; Mishev & Usoskin, 2018).

In CRAC:DOMO, the effective dose in (Sv h^{-1}) (after the integration to 1 hr over time of Equation 3) at a given atmospheric altitude (depth) h is computed by integral product of the prescribed CR spectrum with the corresponding yield function for the given atmospheric depth:

$$E(h,T,\theta,\varphi) = \sum_i \int_{T(R_c)}^{\infty} \int_{\Omega} J_i(T) \cdot Y_i(T,h,\theta,\phi)\, d\Omega(\theta,\varphi)\, dT, \quad (3)$$

where $J_i(T)$ is the differential energy spectrum of CRs at the top of the atmosphere [cm^{-2} s^{-1} sr^{-1} GeV^{-1} nucleon] (for the i−th component: proton or α-particle) with Y_i the dose yield function (Sv cm^2 sr $nucleon^{-1}$). The integration is over the kinetic energy above $T(R_c)$, which is defined by the local cut-off rigidity R_c and over the solid angle Ω. The effective dose yield function Y_i (Sv cm^2 sr $nucleon^{-1}$) is defined as:

$$Y_i(T,h,\theta,\phi) = \sum_j \int_{T^*} F_{i,j}(h,T,T^*,\theta,\phi) \cdot C_j(T^*)\, dT^* \quad (4)$$

where $C_j(T^*)$ is the fluence to effective dose conversion coefficient for a secondary particle of type j (neutron, proton, γ, e^-, e^+, μ^-, μ^+, π^-, π^+) with energy T^*, $F_{i,j}(h,T,T^*,\theta,\varphi)$ is the fluence of secondary particles of type j with energy T^*, produced by a primary CR particle of type i (proton or α-particle) with a given primary energy T arriving at the top of the atmosphere from zenith angle θ and azimuth angle φ. The model also accounts for heavy CR nuclei similarly to Usoskin and Kovaltsov (2006), that is, by scaling them to α-particles. We note that the solid angle integration is straightforward for GCRs, considering their omnidirectional flux, whilst for SEPs, a vertical incidence is routinely assumed, which provides a conservative estimate of the overall dose (Dorman, 2004; Miroshnichenko, 2018), and is consistent with particle propagation in the interplanetary space (Waterfall et al., 2022). In CRAC:DOMO, the total dose can be calculated as a superposition of the dose produced by GCRs and SEPs, with their own respective spectra inputs.

The GCR spectrum was modeled using the force-field model (Caballero-Lopez & Moraal, 2004; Gleeson & Axford, 1968; Usoskin et al., 2005), which uses a single solar modulation potential parameter (ϕ) to analytically modulate the local interstellar spectra of GCRs. For the latter, we used the estimate by Vos and Potgieter (2015). In this work, moderate solar activity is assumed, and ϕ is set to 500 MV.

In this work, the SEP spectra inputted into CRAC:DOMO were derived using measurements from the neutron monitor network to reconstruct the spectra and angular distributions that best reproduce the global neutron monitor network response (for details see Mishev, Tuohino et al., 2018; Mishev, Usoskin et al., 2018). Herein, we employed the spectra obtained during the strongest observed GLE (GLE #5) (Asvestari et al., 2017; Usoskin et al., 2020), which occurred on 23-Feb-1956. GLE #5 is taken in this work as a hypothetical, realistic, strong SEP event and was applied during the effective dose computations for the globe and selected flights, under the differing geomagnetic conditions. The SEP time-dependent spectra during GLE #5 were derived in a recent work (Hayakawa et al., 2024).

5. Results

The total (flight-integrated) doses along the two selected flight paths were computed using cut-off rigidities derived at each 100-year interval over the Laschamps excursion, as outlined above. The CRAC:DOMO inputs for the GCR background were kept identical between computations ($\phi = 500$ MV), with the only difference being the cut-off rigidity along the two flight paths being affected by the changing geomagnetic field. Figure 3 shows the total effective dose produced by background GCRs in comparison to the baseline dose computed for the same flights under modern conditions. Figure 4 is similar to Figure 3, however, the aforementioned spectra for GLE #5 were applied 2 hrs into each flight. The time of the sudden onset of the GLE was set as 16:00 UTC, assuming both flights started at 14:00 UTC. 16:00 UTC was selected so that the majority of the GLE was captured during the middle of the flight, the main phase of GLE #5 being around 4 hr long. We also assumed a conservative approach, namely an isotropic angular distribution of the SEP flux similar to Copeland et al. (2018) and constant altitude during the flight of about 40 kft. The doses significantly changed over the Laschamps excursion, indicating changing levels of geomagnetic shielding over the flight paths as a result of the distortion of the geomagnetic field.

Under modern-day conditions, approximately 13.6% of the Earth is covered in "low-cut-off regions." For the context of this work, low-cut-off regions are defined as regions where the local geomagnetic cut-off is less than

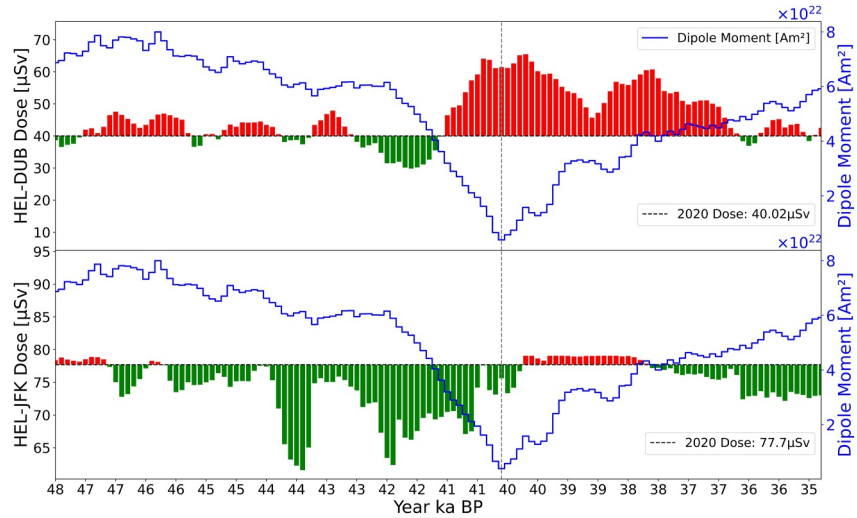

Figure 3. Comparison of total effective dose over the two flight paths throughout the Laschamps excursion, at 100-year intervals, and 2020 epoch at 40 kft due to GCRs. Red indicates an increase in the total dose over the 2020 flight, and green indicates a decrease. The blue line indicates the Earth's dipole moment. The gray dashed vertical line highlights the deepest phase of the Laschamps excursion at 40950 BP, corresponding with the minimum value of the dipole moment. Top: Helsinki to Dubai flight. Bottom: Helsinki to New York flight.

the typical polar atmospheric cut-off energy at sea level (410–430 MeV), (for details see Poluianov & Batalla, 2022; Rishbeth et al., 2009). Note, the atmospheric cut-off varies as a function of altitude; the polar sea-level atmospheric cut-off is taken here as a rough indicator of low-cut-off regions. Accordingly, "low-cut-off regions" are defined in this study as regions with $R_c < 1$ GV.

Total global coverage of low-cut-off regions throughout the Laschamps excursion can be seen in Figure 5. An increase, by a factor of >3 versus the present-day condition, in low-cut-off region coverage is observed around the deep phase of the excursion. It is natural to conclude, therefore, that, globally, atmospheric radiation levels increase in tandem with low-cut-off region coverage; however, the configuration of the geomagnetic shielding is crucial when evaluating CR-induced effects. This is readily apparent in Figures 3 and 4, where the total dose of the HEL-JFK transpolar flight route decreases in relation to the modern epoch during the excursion deep phase

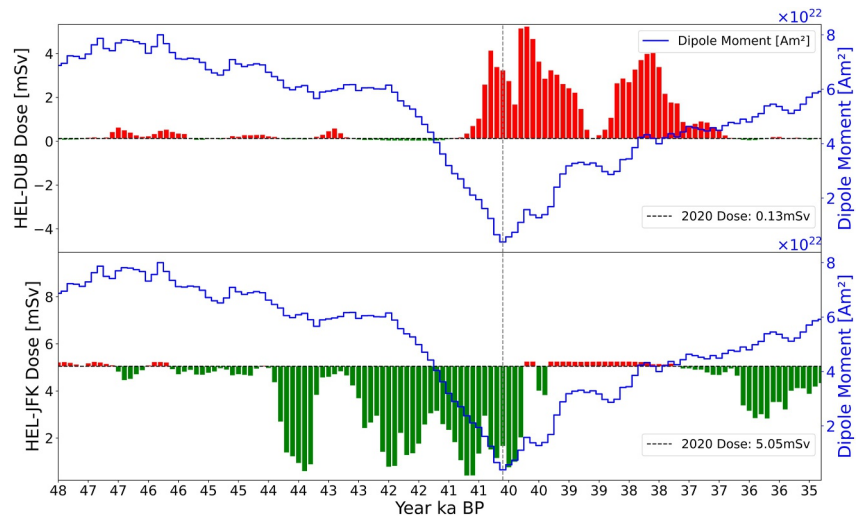

Figure 4. Same as Figure 3, but a hypothetical GLE was applied 2 hr into each flight in addition to the GCR impact. The total dose is thus the combined result of SEP and GCR contributions. GLE #5 was used as a strong, yet realistic scenario in this case.

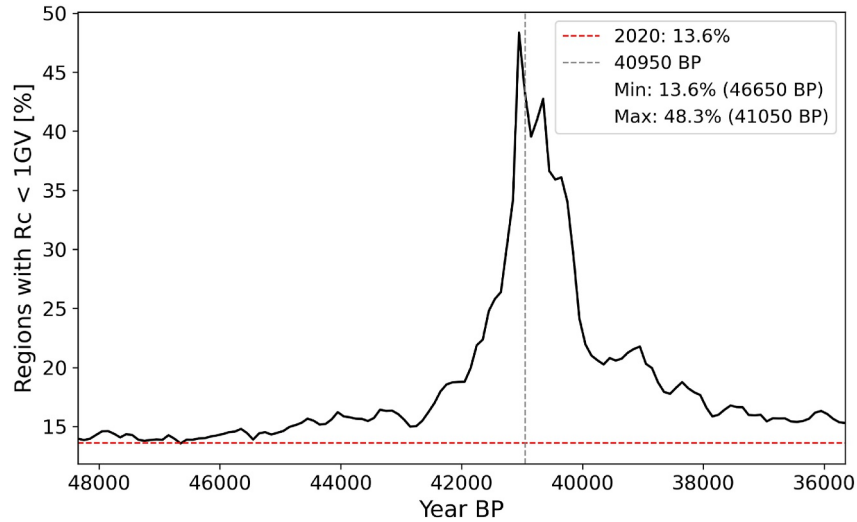

Figure 5. Percentage of the Earth with cut-off values less than 1 GV. The vertical gray line indicates the deep phase of the Laschamps excursion. The red line represents the corresponding percentage for the 2020 epoch.

despite the increase in low-cut-off coverage. Comparison between Figures 1 and 2 reveals that modern regions of low cut-off rigidity can experience increases in geomagnetic shielding while the geomagnetic field weakens during the excursion.

Figure 6 shows the total event integrated effective dose at 40 kft (12.19 km) during the deep phase of the Laschamps excursion when applying the reconstructed GLE #5 SEP spectra as mentioned prior. The peak event integrated dose for the GLE #5 scenario was 4.5 mSv, which is ×4.5 and ×1.5 the average annual dose for the general public and aircrew, 1 and 3 mSv, respectively (EURATOM, 2014). The EURATOM (2014) recommended accumulated annual dose limit for aircrew is 6 mSv, after which measures should be taken to minimize further exposure. As such, the exposure caused by GLE #5 would amount to roughly 75% of this limit in only 4 hr. We note that other regulatory bodies have higher annual dose limits, such as the ICRP, which sets its limit at 20 mSv per year (ICRP, 2007). The EURATOM (2014) 6 mSv recommendation is used here to allow a conservative assessment of the potential radiological impacts. The electronic supplement also provides a figure for the effective dose for GLE #5 under the modern geomagnetic configuration, where higher doses are limited to the

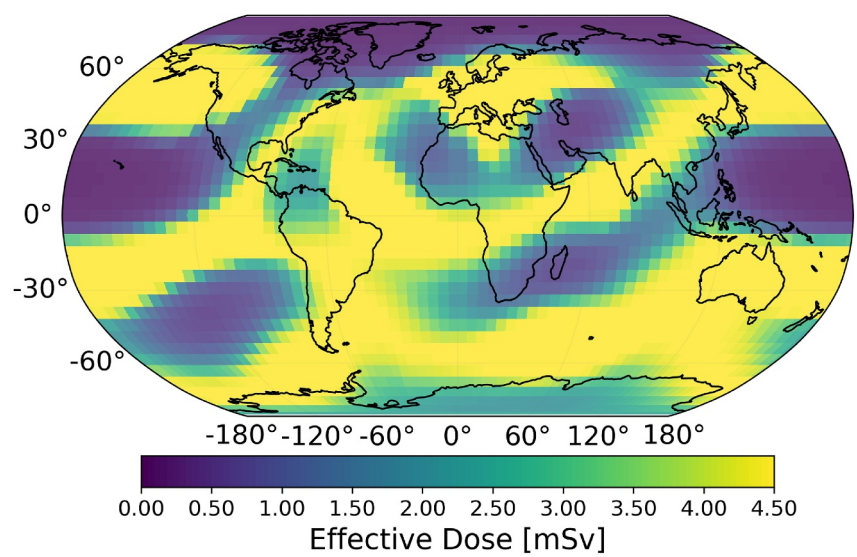

Figure 6. GLE #5 first 4-hr event integrated effective dose at 40 kft if applied to the deep phase of the Laschamps excursion.

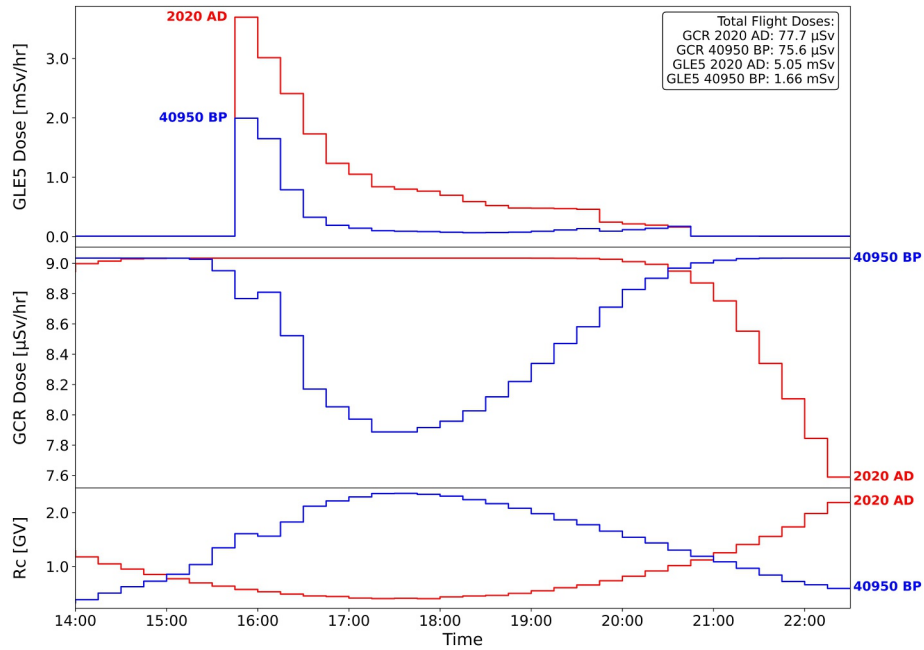

Figure 7. Effective dose rates and cut-off rigidities for a Helsinki to New York flight at 40 kft under two epochs, 2020 AD (red) and 40950 BP (blue). Effective dose rates for background GCRs and an applied GLE #5 event commencing 2 hr into the flight. Total accumulated doses for the respective flights are presented in the top right.

polar regions as suggested by the cut-offs in Figure 2. There is also growing interest in the impact of extreme solar particle events (ESPEs), which can be orders of magnitude stronger than observed modern SEP events (Miyake et al., 2012; Usoskin et al., 2023). A brief analysis of the potential impacts of a hypothetical ESPE event during the Laschamps excursion is provided in Appendix B.

Figures 7 and 8 show the dose rates over the two selected flights for the deep phase of the Laschamps excursion and the same flights during the 2020 epoch, alongside their respective cut-off rigidity values throughout the flight. The variation in the cut-off rigidity and its impact on the dose rate being received on the hypothetical flights is readily apparent in these figures. We also observe how the HEL-JFK flight receives higher dose rates during the 2020 epoch in comparison to the deep phase of the Laschamps excursion, which is also observed in Figures 3 and 4.

6. Conclusion and Discussion

This work has resulted in an update to the OTSO tool that now allows for the application of various magnetic models, such as the LSMOD.2 model (Korte et al., 2019) used in this work. Detailed methodology is also provided for investigations into the impact of CRs during periods of significant geomagnetic field weakening. This opens up the possibility of examining other geomagnetic epochs and excursion events, such as the Mono Lake excursion, and the associated CR-induced effects, such as atmospheric ionisation and cosmogenic isotope production.

During the Laschamps excursion, the Earth's magnetic field significantly reduced in strength, and its typical dipole structure was dramatically distorted. This is reflected in the geomagnetic shielding computations throughout the event, which revealed overall weakening of the geomagnetic shielding, with cut-off rigidities at the deep phase of the Laschamps barely reaching up to 4 GV instead of the modern maximum value of 17 GV. A significant increase in global low-cut-off region coverage during the excursion is also noted, with a roughly threefold increase in regions with cut-off rigidity values less than 1 GV around the deep phase of the excursion. This signifies a substantial decrease in shielding and increased access for CRs, amplifying their impacts.

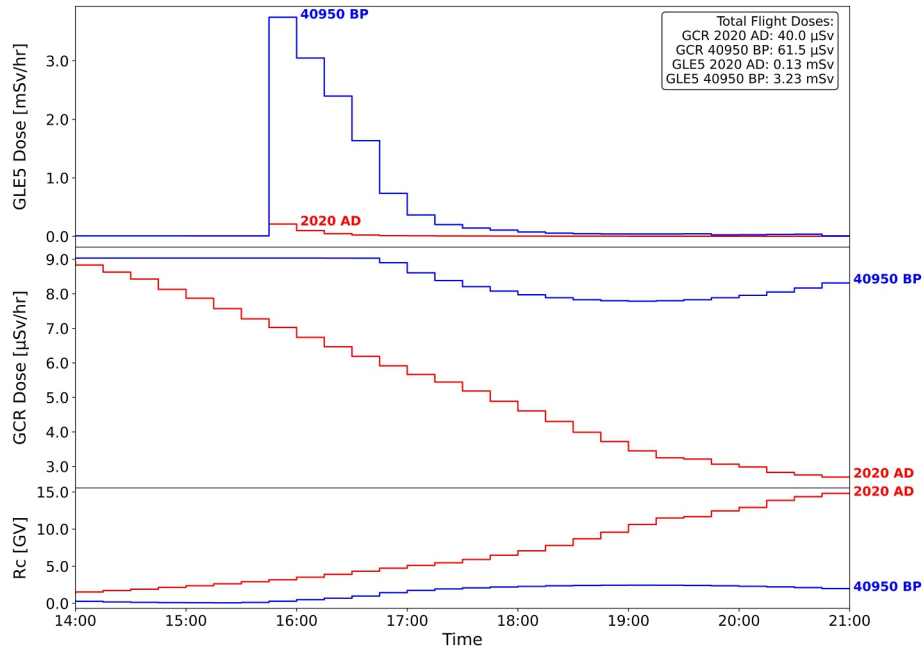

Figure 8. Same as Figure 7 but for a Helsinki to Dubai flight, following the same color scheme for the epochs shown, with 2020 AD (red) and 40950 BP (blue). Flight take-off time and GLE #5 commencement time are identical to those in Figure 7. Accumulated doses for the respective flights are presented in the top right.

The cut-off rigidity computations from this work complement the prior efforts by Gao et al. (2022) by providing cut-off maps with a higher time resolution over the Laschamps excursion; they also independently verify findings that during this event, the difference between vertical and apparent cut-off values is negligible.

Through examining two hypothetical flights throughout the excursion event, it was shown that low-latitude, well-geomagnetically protected flights during the modern era are far more susceptible to CR-induced atmospheric radiation over the Laschamps excursion. Interestingly, the selected high-latitude flight, HEL-JFK, experienced an increase in geomagnetic shielding due to the non-dipole structure of the geomagnetic field; a decrease in the overall dose during the excursion is therefore observed. This can imply that during an excursion, typically safe flight routes can become akin to modern transpolar flight routes. Meanwhile, typically transpolar flights might potentially become preferred for intercontinental travel during an excursion.

Appendix A: Geomagnetic Shielding Results Differences

Figure A1 shows two longitudinal cross-sections of computed geomagnetic cut-off results obtained by Gao et al. (2022) and OTSO. The two longitudes selected highlight two regions where significant differences between the two tools were observed for the 40950 BP epoch, seen in Figure 1. OTSO was used to compute both the apparent and vertical cut-off for a more direct comparison with Gao et al. (2022). The vertical cut-offs were computed with a higher latitude resolution of 1° in order to check for smaller geomagnetic structures that may have been overlooked with the 5° × 5° grid.

Here we note that there is an overall agreement between the two tools and further verify the findings by Gao et al. (2022) that the difference between vertical and apparent cut-off during the excursion event is minimal. We also see significant increases in cut-off values at discrete points within the Gao et al. (2022) results that are incongruous with the OTSO results and do not appear to follow a clear or expected physical trend. The key difference between the tools is the integration method; thus, this is assumed to be the key cause behind the cut-off result disagreements at these locations.

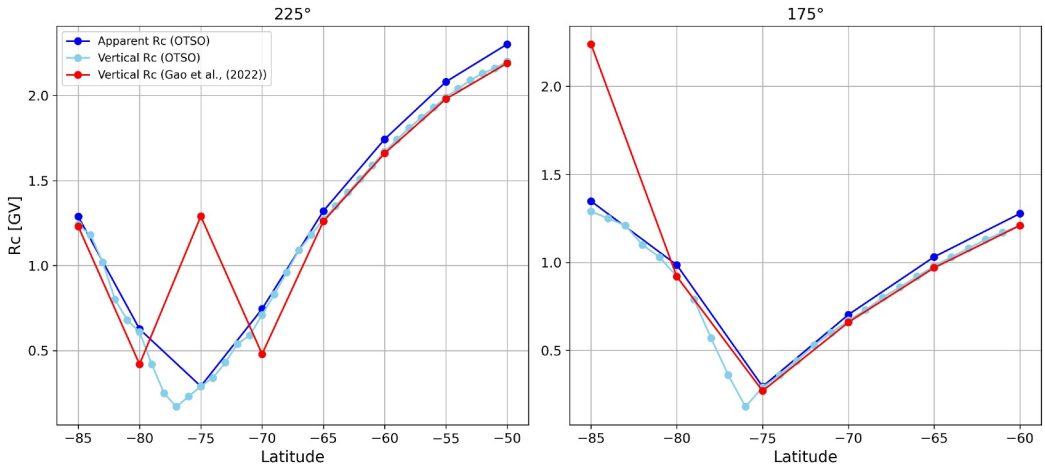

Figure A1. 225° and 175° longitudinal cross-sections of the geomagnetic cut-off rigidities obtained in this work and within Gao et al. (2022).

Appendix B: ESPE/Miyake Event Scenario

In recent years, a new scale of SEP events has been revealed to us through the application of cosmogenic isotope databases, cosmogenic isotopes being isotopes generated via CR interactions in the atmosphere. Looking at the radiocarbon in Japanese tree rings Miyake et al. (2012) discovered a significant, short-lived increase in radiocarbon during 774AD. Initially, several exotic explanations were proposed to account for this increase, including nearby supernovae and gamma-ray bursts. However a solar origin was soon proved (Usoskin et al., 2013), evidenced by factors such as isotope production being higher in the poles (suggesting geomagnetic shielding effects), and derived spectra for these extreme solar particle events (ESPEs), also known as "Miyake events", to be consistent with modern SEP events (for details see Usoskin et al., 2023, and references therein). Current estimates put the 774 AD ESPE as having a flux 40–100 times larger than the SEP event that generated GLE #5 (Koldobskiy et al., 2023). Adopting the same approach as that performed by Mishev et al. (2023), a worst-case scenario of the radiation dose at an altitude of 40 kft for the 774 AD ESPE was computed using the recently revised GLE #5 spectra scaled by a factor of 100 and applying the event to the deep phase of the Laschamps Excursion, results are presented in Figure B1. The peak effective dose over the course of the Miyake event was 0.45 Sv, which is ×450 and ×150 the

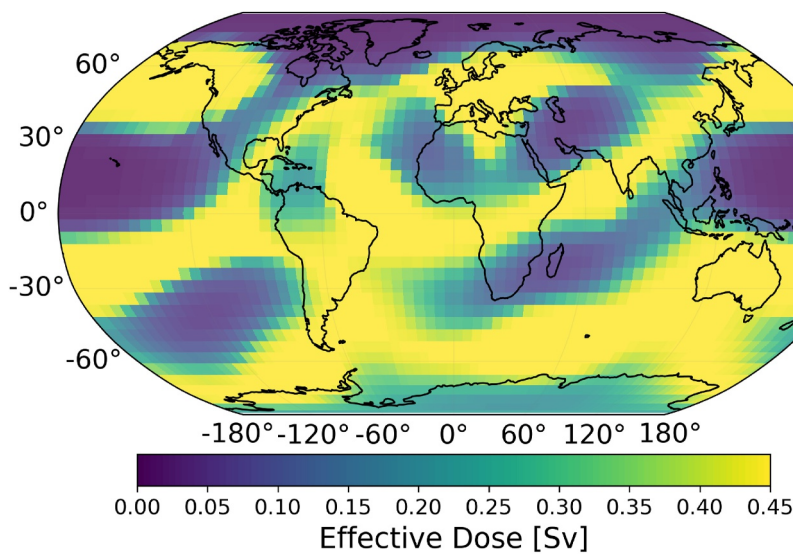

Figure B1. 774 AD event first 4-hr integrated effective dose at 40 kft if applied to the deep phase of the Laschamps excursion. GLE #5 spectra scaled by a factor of 100 were used to represent the ESPE of 774 AD.

average annual dose for the general public and aircrew, 1 and 3 mSv, respectively (EURATOM, 2014). For aircrew, the occupational annual dose limit is recommended to be 6 mSv, the 774 AD Miyake event therefore exceeds this limit by ×75. A similar plot for the impact of the 774 AD ESPE on Earth under the modern geomagnetic configuration is provided in the electronic supplement. An ESPE event with equivalent strength to the 774 AD Miyake event is unlikely to cause immediate radiation sickness-induced fatalities, with acute radiation sickness being observed at a total dose exposure of 1 Sv; however, an absorbed dose of 0.45 Sv in a short timespan can induce mild radiation sickness and dramatically increase the risk of developing cancer (EURATOM, 1996, 2014).

Conflict of Interest

The authors declare no conflicts of interest relevant to this study.

Data Availability Statement

The LSMOD.2 global palaeomagnetic field model is freely available from https://doi.org/10.5880/GFZ.2.3.2019.001 (Korte & Brown, 2019). The latest version of the open-source OTSO tool for global geomagnetic cut-off computations is available from the Zenodo repository (Larsen, 2024). Computed cut-off and effective dose values for the globe and the selected flights over the Laschamps event are included in the electronic supplements and additionally stored in a Zenodo repository (Larsen et al., 2025) for posterity.

Acknowledgments
This work was partly supported by the Research Council of Finland (project 354280) and European Research Council Synergy Grant (project 101166910). This work was also supported by the Transdisciplinary Network linking Space-Earth Environmental Science, History, and Archaeology project (JPMXP1324134720). We acknowledge the support of the International Space Science Institute (Bern, Switzerland) international team No. 585 (REASSESS). The work was partially supported by the Horizon Europe program projects ALBATROS (GA 101077071) and SPEARHEAD (GA 101135044). This work was partially supported by the National Science Fund of Bulgaria under contract KP-06-H64/3. This work was carried out by the joint research program of Institute for Space–Earth Environmental Research, Nagoya University. Open Access funding provided by Nagoya University.

References

Agostinelli, S., Allison, J., Amako, K., Apostolakis, J., Araujo, H., Arce, P., et al. (2003). Geant4—A simulation toolkit. *Nuclear Instruments and Methods in Physics Research Section A: Accelerators, Spectrometers, Detectors and Associated Equipment*, *506*(3), 250–303. https://doi.org/10.1016/S0168-9002(03)01368-8

Alken, P., Thébault, E., Beggan, C. D., Amit, H., Aubert, J., Baerenzung, J., et al. (2021). International geomagnetic reference field: The thirteenth generation. *Earth Planets and Space*, *73*(1), 49. https://doi.org/10.1186/s40623-020-01288-x

Arsenović, P., Rozanov, E., Usoskin, I., Turney, C., Sukhodolov, T., McCracken, K., et al. (2024). Global impacts of an extreme solar particle event under different geomagnetic field strengths. *Proceedings of the National Academy of Sciences*, *121*(28), e2321770121. https://doi.org/10.1073/pnas.2321770121

Aschwanden, M. (2012). GEV particle acceleration in solar flares and ground level enhancement (GLE) events. *Space Science Reviews*, *171*(1–4), 3–21. https://doi.org/10.1007/s11214-011-9865-x

Asvestari, E., Willamo, T., Gil, A., Usoskin, I., Kovaltsov, G., Mikhailov, V., & Mayorov, A. (2017). Analysis of ground level enhancements (GLE): Extreme solar energetic particle events have hard spectra. *Advances in Space Research*, *60*(4), 781–787. https://doi.org/10.1016/j.asr.2016.08.043

Beck, P. (2009). Overview of research on aircraft crew dosimetry during the last solar cycle. *Radiation Protection Dosimetry*, *136*(4), 244–250. https://doi.org/10.1093/rpd/ncp158

Bieber, J. W., Clem, J., & Evenson, P. (1997). Efficient computation of apparent cutoffs. In *International Cosmic Ray Conference* (Vol. 2, p. 389).

Brown, M., Korte, M., Holme, R., Wardinski, I., & Gunnarson, S. (2018). Earth's magnetic field is probably not reversing. *Proceedings of the National Academy of Sciences*, *115*(20), 5111–5116. https://doi.org/10.1073/pnas.1722110115

Buffett, B. A. (2000). Earth's core and the geodynamo. *Science*, *288*(5473), 2007–2012. https://doi.org/10.1126/science.288.5473.2007

Bütikofer, R. (2018). *Cosmic ray particle transport in the Earth's magnetosphere*. (pp. 79–94). Springer International Publishing. https://doi.org/10.1007/978-3-319-60051-2_5

Caballero-Lopez, R., & Moraal, H. (2004). Limitations of the force field equation to describe cosmic ray modulation. *Journal of Geophysical Research*, *109*, A01101. https://doi.org/10.1029/2003JA010098

Cliver, E. W., Schrijver, C. J., Shibata, K., & Usoskin, I. G. (2022). Extreme solar events. *Living Reviews in Solar Physics*, *19*(1), 2. https://doi.org/10.1007/s41116-022-00033-8

Constable, C., Korte, M., & Panovska, S. (2016). Persistent high paleosecular variation activity in southern hemisphere for at least 10000 years. *Earth and Planetary Science Letters*, *453*, 78–86. https://doi.org/10.1016/j.epsl.2016.08.015

Cooke, D., Humble, J., Shea, M., Smart, D., Lund, N., Rasmussen, I., et al. (1991). On cosmic-ray cutoff terminology. *Il Nuovo Cimento—B C*, *14*(3), 213–234. https://doi.org/10.1007/bf02509357

Copeland, K., Matthiä, D., & Meier, M. (2018). Solar cosmic ray dose rate assessments during GLE 72 using MIRA and Pandoca. *Space Weather*. in press. https://doi.org/10.1029/2018SW001917

Copeland, K., Sauer, H., Duke, F., & Friedberg, W. (2008). Cosmic radiation exposure of aircraft occupants on simulated high-latitude flights during solar proton events from 1 January 1986 through 1 January 2008. *Advances in Space Research*, *42*(6), 1008–1029. https://doi.org/10.1016/j.asr.2008.03.001

Desai, M., & Giacalone, J. (2016). Large gradual solar energetic particle events. *Living Reviews in Solar Physics*, *13*(1), 3. https://doi.org/10.1007/s41116-016-0002-5

Desorgher, L., Flückiger, E., Gurtner, M., Moser, M., & Bütikofer, R. (2005). A Geant 4 code for computing the interaction of cosmic rays with the Earth's atmosphere. *International Journal of Modern Physics A*, *20*(A11), 6802–6804. https://doi.org/10.1142/S0217751X05030132

Dorman, L. (2004). *Cosmic rays in the earth's atmosphere and underground*. Kluwer Academic Publishers.

EURATOM. (1996). Council directive 96/29/euratom of 13 May 1996 laying down basic safety standards for protection of the health of workers and the general public against the dangers arising from ionising radiation. *Official Journal of the European Communities*, *39*(L159).

EURATOM. (2014). Directive 2013/59/euratom of 5 December 2013 laying down basic safety standards for protection against the dangers arising from exposure to ionising radiation, and repealing directives 89/618/euratom, 90/641/euratom, 96/29/euratom, 97/43/euratom and 2003/122/euratom. *Official Journal of the European Communities*, *57*(L13).

Gaisser, T., Engel, R., & Resconi, E. (2016). *Cosmic rays and particle physics*. Cambridge University Press.
Gao, J., Korte, M., Panovska, S., Rong, Z., & Wei, Y. (2022). Effects of the Laschamps excursion on geomagnetic cutoff rigidities. *Geochemistry, Geophysics, Geosystems*, *23*(2), e2021GC010261. https://doi.org/10.1029/2021GC010261
Gerontidou, M., Katzourakis, N., Mavromichalaki, H., Yanke, V., & Eroshenko, E. (2021). World grid of cosmic ray vertical cut-off rigidity for the last decade. *Advances in Space Research*, *67*(7), 2231–2240. https://doi.org/10.1016/j.asr.2021.01.011
Gleeson, L. J., & Axford, W. I. (1968). Solar modulation of galactic cosmic rays. *The Astrophysical Journal*, *154*, 1011. https://doi.org/10.1086/149822
Gopalswamy, N., Xie, H., Akiyama, S., Mäkelä, P., & Yashiro, S. (2014). Major solar eruptions and high-energy particle events during solar cycle 24. *Earth Planets and Space*, *66*(1), 104. https://doi.org/10.1186/1880-5981-66-104
Gopalswamy, N., Xie, H., Yashiro, S., Akiyama, S., Mäkelä, P., & Usoskin, I. (2012). Properties of ground level enhancement events and the associated solar eruptions during solar cycle 23. *Space Science Reviews*, *171*(1–4), 23–60. https://doi.org/10.1007/s11214-012-9890-4
Guillou, H., Singer, B. S., Laj, C., Kissel, C., Scaillet, S., & Jicha, B. R. (2004). On the age of the Laschamp geomagnetic excursion. *Earth and Planetary Science Letters*, *227*(3–4), 331–343. https://doi.org/10.1016/j.epsl.2004.09.018
Hands, A., Lei, F., Davis, C., Clewer, B., Dyer, C., & Ryden, K. (2022). A new model for nowcasting the aviation radiation environment with comparisons to in situ measurements during GLES. *Space Weather*, *20*(8), e2022SW003155. https://doi.org/10.1029/2022SW003155
Hayakawa, H., Koldobskiy, S., Mishev, A., Poluianov, S., Gil, A., Usoskina, I., & Usoskin, I. (2024). Revision of the strongest solar energetic particle event of 23 February 1956 (GLE #5) based on the rediscovered original records. *Astronomy & Astrophysics*, *684*, A46. https://doi.org/10.1051/0004-6361/202348699
ICRP. (2007). ICRP publication 103: The 2007 recommendations of the international commission on radiological protection. *Annals of the ICRP*, *37*(2–4).
Klein, K.-L., & Dalla, S. (2017). Acceleration and propagation of solar energetic particles. *Space Science Reviews*, *212*(3–4), 1107–1136. https://doi.org/10.1007/s11214-017-0382-4
Koldobskiy, S., Mekhaldi, F., Kovaltsov, G., & Usoskin, I. (2023). Multiproxy reconstructions of integral energy spectra for extreme solar particle events of 7176 BCE, 660 BCE, 775 CE and 994 CE. *Journal of Geophysical Research: Space Physics*, *128*(3), e2022JA031186. https://doi.org/10.1029/2022JA031186
Korte, M., & Brown, M. (2019). LSMOD.2 — Global paleomagnetic field model for 50–30 ka BP [Dataset]. *GFZ Data Services*. https://doi.org/10.5880/GFZ.2.3.2019.001
Korte, M., Brown, M. C., Panovska, S., & Wardinski, I. (2019). Robust characteristics of the Laschamp and mono lake geomagnetic excursions: Results from global field models. *Frontiers in Earth Science*, *7*, 86. https://doi.org/10.3389/feart.2019.00086
Kruchinin, P. A., Malakhov, V. V., Golubkov, V. S., & Mayorov, A. G. (2024). Calculation of geomagnetic cutoff rigidity using tracing based on the Buneman–Boris method. *Geomagnetism and Aeronomy*, *64*(5), 735–742. https://doi.org/10.1134/S0016793224600668
Larsen, N. (2024). NLarsen15/OTSO: Otso [Software]. *Zenodo*. https://doi.org/10.5281/zenodo.7380188
Larsen, N., & Mishev, A. (2023). Analysis of the ground level enhancement GLE 60 on 15 April 2001, and its space weather effects: Comparison with dosimetric measurements. *Space Weather*, *21*(8), e2023SW003488. https://doi.org/10.1029/2023SW003488
Larsen, N., & Mishev, A. (2024). Relationship between nm data and radiation dose at aviation altitudes during GLE events. *Space Weather*, *22*(6), e2024SW003885. https://doi.org/10.1029/2024SW003885
Larsen, N., & Mishev, A. (2025). Radiation impact of the Halloween GLE events during the October–November 2003 period. *Space Weather*, *23*(1), e2024SW004199. https://doi.org/10.1029/2024SW004199
Larsen, N., Mishev, A., & Usoskin, I. (2023). A new open-source geomagnetosphere propagation tool (OTSO) and its applications. *Journal of Geophysical Research: Space Physics*, *128*(3), e2022JA031061. https://doi.org/10.1029/2022JA031061
Larsen, N., Usoskin, I., Mishev, A., Koldobskiy, S., & Väisänen, P. (2025). Reduced geomagnetic shielding during the Laschamps excursion and its impact on cosmic-ray-induced atmospheric radiation—Dataset [Dataset]. *Zenodo*. https://doi.org/10.5281/zenodo.17173159
Latocha, M., Beck, P., & Rollet, S. (2009). Avidos-a software package for European accredited aviation dosimetry. *Radiation Protection Dosimetry*, *136*(4), 286–290. https://doi.org/10.1093/rpd/ncp126
Matthiä, D., Sihver, L., & Meier, M. (2008). Monte-Carlo calculations of particle fluences and neutron effective dose rates in the atmosphere. *Radiation Protection Dosimetry*, *131*(2), 222–228. https://doi.org/10.1093/rpd/ncn130
Meier, M., Copeland, K., Matthiä, D., Mertens, C. J., & Schennetten, K. (2018). First steps toward the verification of models for the assessment of the radiation exposure at aviation altitudes during quiet space weather conditions. *Space Weather*, *16*(9), 1269–1276. https://doi.org/10.1029/2018SW001984
Meier, M., Trompier, F., Ambrozova, I., Kubancak, J., Matthiä, D., Ploc, O., et al. (2016). Concord: Comparison of cosmic radiation detectors in the radiation field at aviation altitudes. *Journal of Space Weather and Space Climate*, *6*, A24. https://doi.org/10.1051/swsc/2016017
Mertens, C., Gronoff, G., & Phoenix, D. (2025). Nairas version 3 atmospheric ionizing radiation validation: Comparisons to rad-x measurements. *Space Weather*, *23*(4), e2024SW004296. https://doi.org/10.1029/2024SW004296
Mertens, C., Meier, M., Brown, S., Norman, R., & Xu, X. (2013). Nairas aircraft radiation model development, dose climatology, and initial validation. *Space Weather*, *11*(10), 603–635. https://doi.org/10.1002/swe.20100
Miroshnichenko, L. (2018). Retrospective analysis of GLES and estimates of radiation risks. *Journal of Space Weather and Space Climate*, *8*, A52. https://doi.org/10.1051/swsc/2018042
Mishev, A., Binios, A., Turunen, E., Leppänen, A.-P., Larsen, N., Tanskanen, E., et al. (2022). Measurements of natural radiation with an Mdu Liulin type device at ground and in the atmosphere at various conditions in the arctic region. *Radiation Measurements*, *154*, 106757. https://doi.org/10.1016/j.radmeas.2022.106757
Mishev, A., Koldobskiy, S., Usoskin, I., Kocharov, L., & Kovaltsov, G. (2021). Application of the verified neutron monitor yield function for an extended analysis of the GLE # 71 on 17 May 2012. *Space Weather*, *19*(2), e2020SW002626. https://doi.org/10.1029/2020SW002626
Mishev, A., Panovska, S., & Usoskin, I. (2023). Assessment of the radiation risk at flight altitudes for an extreme solar particle storm of 774 ad. *Journal of Space Weather and Space Climate*, *13*, 22. https://doi.org/10.1051/swsc/2023020
Mishev, A., Tuohino, S., & Usoskin, I. (2018a). Neutron monitor count rate increase as a proxy for dose rate assessment at aviation altitudes during GLES. *Journal of Space Weather and Space Climate*, *8*, A46. https://doi.org/10.1051/swsc/2018032
Mishev, A., & Usoskin, I. (2018). Assessment of the radiation environment at commercial jet-flight altitudes during GLE 72 on 10 September 2017 using neutron monitor data. *Space Weather*, *16*(12), 1921–1929. https://doi.org/10.1029/2018SW001946
Mishev, A., Usoskin, I., Raukunen, O., Paassilta, M., Valtonen, E., Kocharov, L., & Vainio, R. (2018b). First analysis of GLE 72 event on 10 September 2017: Spectral and anisotropy characteristics. *Solar Physics*, *293*, 136. https://doi.org/10.1007/s11207-018-1354-x
Mishev, A., & Velinov, P. (2014). Influence of hadron and atmospheric models on computation of cosmic ray ionization in the atmosphere-extension to heavy nuclei. *Journal of Atmospheric and Solar-Terrestrial Physics*, *120*, 111–120. https://doi.org/10.1016/j.jastp.2014.09.007

Mishev, A., & Usoskin, I. (2015). Numerical model for computation of effective and ambient dose equivalent at flight altitudes: Application for dose assessment during GLES. *Journal of Space Weather and Space Climate*, *5*(3), A10. https://doi.org/10.1051/swsc/2015011
Miyake, F., Nagaya, K., Masuda, K., & Nakamura, T. (2012). A signature of cosmic-ray increase in AD 774-775 from tree rings in Japan. *Nature*, *486*(7402), 240–242. https://doi.org/10.1038/nature11123
Mukhopadhyay, A., Panovska, S., Garvey, R., Liemohn, M. W., Ganjushkina, N., Brenner, A., et al. (2025). Wandering of the auroral oval 41,000 years ago. *Science Advances*, *11*(16), eadq7275. https://doi.org/10.1126/sciadv.adq7275
Panovska, S., Constable, C. G., & Korte, M. (2018). Extending global continuous geomagnetic field reconstructions on timescales beyond human civilization. *Geochemistry, Geophysics, Geosystems*, *19*(12), 4757–4772. https://doi.org/10.1029/2018GC007966
Panovska, S., Korte, M., & Constable, C. (2019). One hundred thousand years of geomagnetic field evolution. *Reviews of Geophysics*, *57*(4), 1289–1337. https://doi.org/10.1029/2019RG000656
Panovska, S., Korte, M., Liu, J., & Nowaczyk, N. (2021). Global evolution and dynamics of the geomagnetic field in the 15–70 kyr period based on selected paleomagnetic sediment records. *Journal of Geophysical Research: Solid Earth*, *126*(12), e2021JB022681. https://doi.org/10.1029/2021JB022681
Papaioannou, A., Strauss, R. D. T., Lario, D., Vainio, R., Wijsen, N., Afanasiev, A., et al. (2025). Predicting solar energetic particles: Solar storm watch—Preparing for space odyssey. *Space Science Reviews*, *221*(6), 82. https://doi.org/10.1007/s11214-025-01211-4
Pelliccioni, M. (2000). Overview of fluence-to-effective dose and fluence-to-ambient dose equivalent conversion coefficients for high energy radiation calculated using the Fluka code. *Radiation Protection Dosimetry*, *88*(4), 279–297. https://doi.org/10.1093/oxfordjournals.rpd.a033046
Petoussi-Henss, N., Bolch, W., Eckerman, K., Endo, A., Hertel, N., Hunt, J., et al. (2010). Conversion coefficients for radiological protection quantities for external radiation exposures. *Annals of the ICRP*, *40*(2–5), 1–257. https://doi.org/10.1016/j.icrp.2011.10.001
Poluianov, S., & Batalla, O. (2022). Cosmic-ray atmospheric cutoff energies of polar neutron monitors. *Advances in Space Research*, *70*(9), 2610–2617. https://doi.org/10.1016/j.asr.2022.03.037
Poluianov, S., Usoskin, I., Mishev, A., Shea, M., & Smart, D. (2017). GLE and sub-GLE redefinition in the light of high-altitude polar neutron monitors. *Solar Physics*, *292*(11), 176. https://doi.org/10.1007/s11207-017-1202-4
Potgieter, M. (2013). Solar modulation of cosmic rays. *Living Reviews in Solar Physics*, *10*(3). https://doi.org/10.12942/lrsp-2013-3
Pulkkinen, T. (2007). Space weather: Terrestrial perspective. *Living Reviews in Solar Physics*, *4*(1), 1–60. https://doi.org/10.12942/lrsp-2007-1
Ripperda, B., Bacchini, F., Teunissen, J., Xia, C., Porth, O., Sironi, L., et al. (2018). A comprehensive comparison of relativistic particle integrators. *The Astrophysical Journal—Supplement Series*, *235*(1), 21. https://doi.org/10.3847/1538-4365/aab114
Rishbeth, H., Shea, M., & Smart, D. (2009). The solar-terrestrial event of 23 February 1956. *Advances in Space Research*, *44*(10), 1096–1106. https://doi.org/10.1016/j.asr.2009.06.020
Roberts, A. P. (2008). Geomagnetic excursions: Knowns and unknowns. *Geophysical Research Letters*, *35*(17). https://doi.org/10.1029/2008GL034719
Sato, T., Yasuda, H., Niita, K., Endo, A., & Sihver, L. (2008). Development of Parma: Phits-based analytical radiation model in the atmosphere. *Radiation Research*, *170*(2), 244–259. https://doi.org/10.1667/rr1094.1
Schmidt, A. (1917). Erdmagnetismus. *Encyklopädie der mathematischen Wissenschaften mit Einschluss ihrer Anwendungen*, *6*, 265–396.
Shea, M., & Smart, D. (1982). Possible evidence for a rigidity-dependent release of relativistic protons from the solar corona. *Space Science Reviews*, *32*(1–2), 251–271. https://doi.org/10.1007/BF00225188
Shea, M., & Smart, D. (2000). Fifty years of cosmic radiation data. *Space Science Reviews*, *93*(1–2), 229–262. https://doi.org/10.1023/A:1026500713452
Shea, M., & Smart, D. (2012). Space weather and the ground-level solar proton events of the 23rd solar cycle. *Space Science Reviews*, *171*(1), 161–188. https://doi.org/10.1007/s11214-012-9923-z
Shea, M., Smart, D., & McCracken, K. (1965). A study of vertical cut off rigidities using sixth degree simulations of the geomagnetic field. *Journal of Geophysical Research*, *70*(17), 4117–4130. https://doi.org/10.1029/jz070i017p04117
Smart, D., & Shea, M. (2001). *Geomagnetic cutoff rigidity computer program: Theory, software description and example*. NASA STI/Recon Technical Report N.
Spurny, F., Votockova, I., & Bottollier-Depois, J. (1996). Geographical influence on the radiation exposure of an aircrew on board a subsonic aircraft. *Radioprotection*, *31*(2), 275–280.
Stoer, J., & Bulirsch, R. (2002). *Introduction to numerical analysis* (Vol. 12). Springer Science & Business Media.
Usoskin, I., Alanko-Huotari, K., Kovaltsov, G., & Mursula, K. (2005). Heliospheric modulation of cosmic rays: Monthly reconstruction for 1951–2004. *Journal of Geophysical Research*, *110*(A12108). https://doi.org/10.1029/2005JA011250
Usoskin, I., Miyake, F., Baroni, M., Brehm, N., Dalla, S., Hayakawa, H., et al. (2023). Extreme solar events: Setting up a paradigm. *Space Science Reviews*, *219*(8), 73. https://doi.org/10.1007/s11214-023-01018-1
Usoskin, I. G., Koldobskiy, S. A., Kovaltsov, G. A., Rozanov, E. V., Sukhodolov, T. V., Mishev, A. L., & Mironova, I. A. (2020). Revisited reference solar proton event of 23 February 1956: Assessment of the cosmogenic-isotope method sensitivity to extreme solar events. *Journal of Geophysical Research: Space Physics*, *125*(6), e2020JA027921. https://doi.org/10.1029/2020JA027921
Usoskin, I. G., & Kovaltsov, G. A. (2006). Cosmic ray induced ionization in the atmosphere: Full modeling and practical applications. *Journal of Geophysical Research*, *111*(D21), D21206. https://doi.org/10.1029/2006JD007150
Usoskin, I. G., Kovaltsov, G. A., & Mishev, A. L. (2024). Updated model of cosmic-ray-induced ionization in the atmosphere (CRAC:CRII_v3): Improved yield function and lookup tables. *Journal of Space Weather and Space Climate*, *14*, 20. https://doi.org/10.1051/swsc/2024020
Usoskin, I. G., Kromer, B., Ludlow, F., Beer, J., Friedrich, M., Kovaltsov, G. A., et al. (2013). The AD775 cosmic event revisited: The sun is to blame. *Astronomy and Astrophysics*, *552*, L3. https://doi.org/10.1051/0004-6361/201321080
Vay, J.-L. (2008). Simulation of beams or plasmas crossing at relativistic velocity). *Physics of Plasmas*, *15*(5), 056701. https://doi.org/10.1063/1.2837054
Vos, E., & Potgieter, M. (2015). New modeling of galactic proton modulation during the minimum of solar cycle 23/24. *The Astrophysical Journal*, *815*, 119. https://doi.org/10.1088/0004-637X/815/2/119
Waterfall, C. O. G., Dalla, S., Laitinen, T., Hutchinson, A., & Marsh, M. (2022). Modeling the transport of relativistic solar protons along a heliospheric current sheet during historic GLE events. *The Astrophysical Journal*, *934*(1), 82. https://doi.org/10.3847/1538-4357/ac795d
Wissing, J., & Kallenrode, M.-B. (2009). Atmospheric ionization module Osnabrück (AIMOS): A 3-d model to determine atmospheric ionization by energetic charged particles from different populations. *Journal of Geophysical Research*, *114*(6), A06104.